International Journal of Applied Science and Engineering
2006. 4, 1: 1-19

Design, Fabrication and Characterization of a Spherically Focused Capacitive Air-Coupled Ultrasonic Transducer

Junho Song and D. E. Chimenti*

Center for Nondestructive Evaluation and
Department of Aerospace Engineering
Iowa State University
Ames, IA 50011, USA.

Abstract: We report the development, fabrication, and testing of spherically focused capacitive air-coupled ultrasonic transducers, that need no mirror, zone plate, or similar external device. To achieve native focusing, we have employed a flexible copper/polyimide backplate that permits a conformal fit to a spherical fixture whose radius determines the focal length. A spherically deformed aluminized Mylar foil, conforms to the spherical backplate, completing the transducer. Two devices have been fabricated and tested, one having a 1-cm diameter and 2.54-cm focus, and another with a 5-cm diameter and 5.1-cm focus. Both devices have frequency spectra centered at 840 kHz with -6 dB points at 310 and 1200 kHz. Using a quasi-point receiver, the beam diameter is found to be 2.7 mm (1-cm device) and 1.32 mm (5-cm device) in the focal plane, when excited with a broadband signal. The monochromatic diffraction behavior of the 1-cm device agrees with model calculations based on a focused piston radiator to within the measurement resolution of about 2%. Features as small as a 250-micron wire have been successfully imaged using the 5-cm devices in a confocal geometry, demonstrating resolution at the diffraction limit for this device. Further examples of defect imaging in honeycomb composites and in wood are also presented.

Keywords: air-coupling; ultrasonics; NDE; capacitive film; transducer; diffraction-limited resolution.

1. Introduction

Ultrasound inspection techniques have been extended in recent years to non-contact and particularly air-coupled sound generation and detection, owing to the significant advantages they promise and to improvements in instrumentation and materials. Attempting to perform ultrasonic measurements in air, however, suffers from poor coupling of ultrasound energy because of the large impedance mismatch between the air and essentially any solid test medium. Liquid coupling is much more efficient because the acoustic impedance of water is much higher than air; in many applications, however, it may not be possible or practical to use a liquid coupling medium to mediate sound transmission to the article under test. Examples of these materials are woods, paper products, porous materials, hot solid materials, or materials whose properties would be compromised by water

* Corresponding author; e-mail:chimenti@iastate.edu
Accepted for Publication: November14, 2005

contact or immersion. Non-contact inspection methods use only gas or air as a coupling medium, so that there are no risks of contamination of the test article. Recently, better technology and understanding of air-coupled methods have encouraged more applications [1-7], despite the large signal-to-noise penalty typically associated with this form of ultrasonic inspection.

Most air-coupled (A/C) ultrasonic methods employ conventional piezoelectric (PZT) transducers, composite piezoelectric elements (with careful impedance matching) or capacitive foil transducers. When a PZT transducer is used in A/C inspection applications, it encounters very large acoustic impedance mismatch at the boundary between the piezoelectric element and the surrounding air or gas boundary, despite heroic attempts at impedance matching. In fact, the acoustic impedance of piezoelectric materials (~30 x 10^6 kg/m^{2}s) used in the conventional ultrasonic transducers is several orders of magnitude larger than that of air (400 kg/m^{2}s). Kelly *et al.* [4] have employed multilayered silicon rubbers as a half wavelength matching layer on a piezoelectric transducer in air. Kraub *et al.* [5] have used a SiO_2-aerogel as an impedance matching layer. Reily and Hayward [6] have improved the impedance matching by using a 1-3 connectivity piezocomposite active element of different piezoceramic fraction, shape and distribution. However, these remedies are optimized for narrow bandwidth operations and required extensive trial-and-errors to be workable for a particular case.

Capacitive ultrasonic transducers consist of a thin metalized polymer membrane and conducting backplate. Compared to the piezoelectric transducers, the capacitive ultrasonic transducers have much smaller acoustic impedance mismatch between the membrane and air, owing to the very small mechanical impedance of a thin membrane. This arrangement makes a capacitive ultrasonic transducer ideal for coupling into air. The surface of the backplate is patterned in a series of holes by roughening [7] or micromachining [8-14] processes. And a metalized polymer membrane is then placed or fabricated on the patterned backplate for both a receiver and transmitter. Applying a transient voltage between the backplate and the grounded metalized surface of the membrane, in the presence of a constant bias voltage, induces vibration of the membrane. The vibration of the membrane generates ultrasound in air. Similarly, receiving the vibrating sound signals is achieved using the same transducer as a reciprocal device.

More recently, the advent of advanced microfabrication techniques has led to simplified backplate fabrication, low manufacturing costs, and better reproducibility. Consequently, many researchers have studied a variety of backplate fabrication techniques and the effect of backplate design parameters, including backplate surface conditions, membrane properties, and bias voltages. Schindel *et al.* [8] have fabricated a backplate on a (100) silicon wafer using a wet-etching microfabrication technique. They have shown that higher bias voltage generates higher signal amplitude and resonant frequency. And a thicker membrane reduces the performance with lower resonant frequency and narrower bandwidth. Haller *et al.* [9] have fabricated a backplate on (100) silicon wafer using surface micromachining techniques. They replace the metalized polymer film with an aluminum coated Si_3N_4 layer directly deposited on a silicon backplate. Ladabaum *et al.* [10] and Jin *et al.* [11] have developed surface micromachined capacitive ultrasonic transducers for air-coupled and water-immersion applications. These transducers show a good response into the few MHz ranges with excellent sensitivities. Carr *et al.* [12] and Suzuki *et al.* [13] have found the high dependence of the resonant frequency and bias voltages on the membrane thickness using V-grooved silicon backplates. Hietanen *et al.* [14] have shown, using a brass backplate, that there is no influence of the hole size on the resonant frequency.

Capacitive A/C transducers have received increased interest because of their higher sensitivity and wide bandwidth. With them, the field has continued to develop and expand applications in various areas, including materials inspection [15-16], characterization [17-20], and ultrasonic imaging [21]. Understandably, research investigations have been performed to provide for A/C ultrasonics the additional extensions that are routine for liquid-coupled inspection. Chief among these is transducer focusing. Commonly, a focused transducer can provide much higher sensitivity than a planar device. And a capacitive A/C transducer provides wideband frequency response and better resolution than a piezoelectric transducer in air. For example, 1 MHz ultrasonic signals have a wavelength of ~ 340 μm in air, where the speed of sound is 340 m/s. With focusing, 1 MHz spot size will be in the order of a wavelength with very high signal intensity in the focal zone, leading to better detection of defects.

However, pursuit of a spherically focused transducer has been hampered by serious technical challenges. A silicon backplate cannot be deformed because brittle silicon wafers would easily fracture. Instead of deforming the backplate, many researchers have tried alternative ways [22-28]. Schindel *et al.* [22] have used a planar transducer and an external focusing element, such as a Fresnel zone plate. Another approach has been tried by Holland *et al.* [19], Gan *et al.* [23] and Hosten and Castaings [24]. They have used an off-axis parabolic mirror as the focusing element. However, this arrangement still leaves one dimension unfocused and provides only limited bandwidth. In addition, the assembled transducer is quite bulky.

Other efforts have been made to manufacture a curved backplate to compensate for the problems induced by using a secondary device such as a zone plate or a mirror. Wang *et al.* [25] have utilized a curved plastic stand as a backplate and a 36-μm thick polyvinylidene diflouride (PVDF) film coated with a 26-μm thick polyester film as a thin membrane. They report resonant frequencies of 59 and 31 kHz for the extensional and flexural bending modes, respectively. Robertson *et al.* [26] have fabricated a cylindrically focused transducer using polished brass as a backplate. And a 3.5-μm thick Mylar film is placed on the brass backplate as a membrane. Although this device shows good line focusing, the performance of the transducer relies on the surface conditions of the polished brass backplate. Hutchins *et al*. [27] have used a conical A/C capacitive transducer for surface imaging. The transducer consists of a polished brass backplate and a 3.5-μm thick Mylar film. The backplate is fabricated using the same techniques demonstrated by Robertson [26]. So the performance is fully dependent on the surface conditions of the polished brass. In addition, it suffers from wrinkles on the Mylar film when these researchers place the Mylar film on the conically shaped brass backplate. Neither transducer has micromachined patterns on the backplate, so that the advantages of a capacitive micromachined transducer are not available in this design. Wong *et al*. [28] utilize the merits of micromachining but employ a very thin silicon backplate, etched to 150 μm using wet etching techniques. Then, it is carefully deformed into a cylindrical shape. However, the thinned silicon wafer is difficult to handle owing to the fragility and brittleness of the silicon. As fabricated, their device leaves one dimension unfocused and still has bandwidth limitations.

Although many research efforts have endeavored to fabricate a *genuine* focused capacitive air-coupled ultrasonic transducer, there has been no evidence of a successful attempt yet. Instead, many of the researchers try alternative routes to simulate a natively focused ultrasonic transducer. The examples of such research have been described. In our research, a spherically focused capacitive air coupled transducer has been designed, fabricated, and tested, using a new flexible backplate material instead of brittle silicon wafer. Because the new material is so flexible, it is easily deformed into a spherical shape in the proposed transducer. To investigate the role of the backplate on the transducer performance, we perform extensive studies on the surface conditions of the backplate by varying design parameters such as the diameter and depth of the patterns, the center-to-center spacing between the patterns, membrane thickness, and bias voltage. Then, one of the design parameters is applied to the proposed transducer. Its performance is fully studied under various experimental conditions.

2. Transducer design

As shown in Figure 1, a capacitive air-coupled ultrasonic transducer consists of seven replaceable components; a backplate, backplate fixture, metalized polymer film, bottom case, outer case, insulator, and top cover. In a backplate, there are fabricated well-defined, micro-machined pits or depressions on the surface, which play a very important role in determining the performance characteristics of the capacitive air - coupled transducer. The pit design we have used is a square grid pattern with a specific center-to-center spacing. One innovation achieved in this research is that we have developed and employed a flexible copper(Cu)/polyimide(PI) backplate in our capacitive air-coupled transducers, instead of using the conventional rigid Si substrate. Utilizing the Cu/PI's flexibility, we can fabricate backplates in any shape, including planar, cylindrical, or spherical.

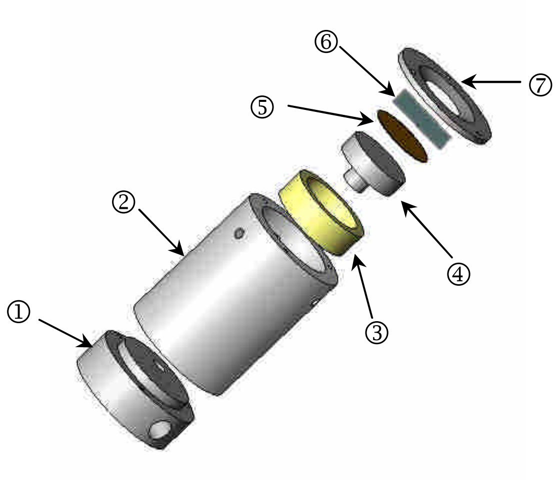

(a)

(b)

Figure 1. (a) Schematic diagram of a capacitive planar air-coupled transducer. (b) A photograph of a fully constructed 10-mm diameter capacitive planar air-coupled transducer. The transducer consists of seven replaceable components: (1) bottom case, (2) outer case, (3) insulator, (4) backplate fixture, (5) backplate, (6) metalized polymer film, and (7) top cover. All the components are aluminum, except the Delrin insulator.

As shown in Figure 1 (a), the backplate (5) is conformed and attached to the backplate fixture (4). Depending on the nature of a capacitive air-coupled transducer, the backplate fixture can be machined in a planar, cylindrical, or spherical shape. For a spherically focused capacitive air-coupled transducer proposed in this research, we use a spherically shaped fixture so that the transducer functions like an ideal spherically focused piston radiator. Because the primary function of the backplate fixture is to provide the backplate with a proper contour for optimal focusing, the requirements of machining precision, specifically surface roughness and dimensional tolerance, are modest.

The backplate fixture is electrically connected to the center pin of a SMA connector mounted on the bottom case, and the shield contact of the SMA connector is connected to the bottom case (1). To isolate the electrical connection between the backplate and the ground, we have added a Delrin insulator (3) between the backplate fixture and the outer case (2). Except the insulator, all the components are fabricated from aluminum.

The last step in the construction process is the installation of a one-sided metalized polymer film (6) placed between the backplate and top cover, with the metalized side facing the top cover. According to several studies [29–31], a metal layer on the metalized polymer film should have a low areal density to lower the film mass and yield higher transducer sensitivity and larger bandwidth. Among many available commercial metalized polymer films we have employed a 6 μm thick PET (Mylar®) film (ρ = 2.56–2.64 g/mm^3) with a 200 nm deposited aluminum coating.

2.1. Principles of operation

The process of generating and receiving ultrasound is very similar to the working principles of a condenser microphone. As shown in Figure 2, a DC bias $V_{dc}(t)$ is superimposed upon a transient voltage signal $V_{ac}(t)$ from a signal source. Electrostatic force attracts the film toward the pits, causing the metalized polymer film to vibrate. The device is reciprocal, receiving the sound waves in air with the same physical principles. In the receiver mode, the received sound waves are transducted into minute capacitance changes, owing to the displacements of the film. The capacitance is converted into electrical signals by the transducer. The dc bias voltage also plays a very important role in determining the performance of a capacitive air-coupled transducer. A complete schematic diagram of the experimental apparatus is shown in Figure 3.

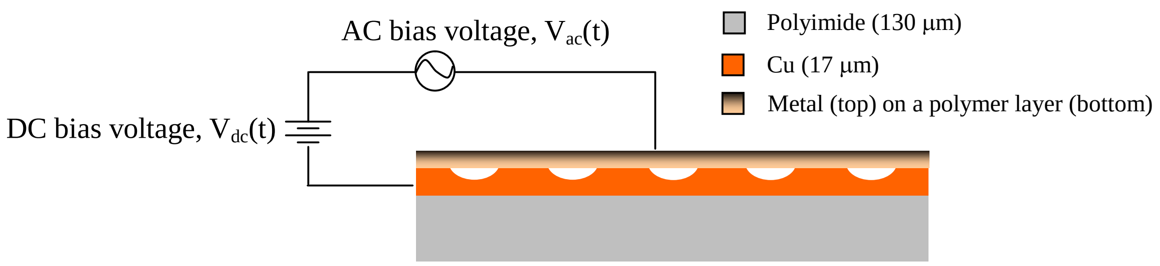

Figure 2. Schematic diagram of a capacitive air-coupled transducer for ultrasound generation in air. The $V_{dc}(t)$ and $V_{ac}(t)$ represent DC bias and AC bias voltages, respectively.

Flexible Cu/PI (RO3003®, Rogers Co.) backplate is made from commonly used printed circuit board (PCB) material. It has a 17-μm thick copper layer deposited on a 130-μm thick polyimide layer. And its surface roughness is measured at approximately ±1.2 μm peak-to-peak using a profilometer. The etched pits show a cupped shape with a 9-μm depth, as shown in Figure 4.

2.2. Signal coding

During the experiments, we strive to obtain measurements with large signal amplitude and high signal-to-noise ratio (SNR). However, air-coupled measurements typically have small signal amplitude and low SNR, which makes it difficult to extract useful information [31]. To enhance the SNR, a pulse compression method has been used. The pulse compression excitation works as follows: suppose a broadband excitation signal is $s(t)$, and the impulse response of a system $h(t)$ is assumed to be linear and time invariant (LTI). Then, the measured signal $r(t)$ is given by

$$r(t) = s(t) * h(t) \tag{1}$$

where '$*$' represents the convolution operator. To find the impulse response $h(t)$ we perform cross-correlation of the excitation signal $s(t)$ with the measured signal $r(t)$. And this is equivalent to convolving (t) with $s(-t)$. Therefore, we can rearrange Equation (1) as

$$r(t) * s(-t) = (s(t) * h(t)) * s(-t). \tag{2}$$

Commuting and associating the right-hand side of Equation (2), we obtain

$$r(t) * s(-t) = (s(t) * s(-t)) * h(t). \tag{3}$$

The result of $s(t) * s(-t)$ is a zero phase signal, which is equivalent to $S(f) * S(f)^*$ in the frequency domain, where the superscript $(\ )^*$ denotes complex conjugation. Note that a broadband signal with zero phase is equivalent to a filtered impulse of the same bandwidth. Therefore, $s(t) * s(-t)$ can be modeled as a band-limited impulse in the time domain, denoted as $\delta(t)$. Therefore, the result of the correlation between measured signal and applied excitation signal is

$$\begin{aligned} r(t) * s(-t) &= \delta(t) * h(t) \\ &= h(t). \end{aligned} \tag{4}$$

That is, we obtain the impulse response of the test medium, limited by the bandwidth tailoring in the choice of the original excitation and the system electronics [19-20].

As mentioned in the Introduction, many unsuccessful attempts have been made to develop focused capacitive film transducers. No one has attempted to fabricate spherical backplates because the silicon typically used as a backplate material is far too brittle. The fabrication of a conformal metalized polymer film is another major obstacle to be overcome in the development of a focused capacitive air-coupled transducer. So, researchers have substituted external devices [22–28]. All these attempts suffer from inherent problems, such as narrowband frequency response and lower sensitivity.

In this research we have designed and tested two sizes of a spherically focused capacitive air-coupled transducer: one has a 10-mm diameter and 25.4-mm geometric focal length; the other has a 50-mm diameter and 50.8-mm geometric focal length. Both transducers employ a flexible copper/polyimide backplate having the same surface geometry, *i.e.* a 40-μm pit diameter, 80-μm center-to-center spacing, and 9-μm pit depth.

3. Transducer fabrication

Our spherically focused capacitive air-coupled transducer devices consist of seven components, shown in Figure 1. In order to simplify references to the 10 mm and 50 mm diameter transducers, we will denote the 10 mm and 50 mm diameter transducers as Type I and Type II transducers, respectively. The spherically curved backplate fixtures for a Type I transducer are machined to have 5±0.1 mm radius of curvature and an active angular sensitivity of ±15° with respect to the normal axis. It is designed to provide approximately 25.4-mm (or 1-inch) geometric focal length, and should be applicable to almost all phase-match angles for common engineering materials, including metals, plastics, and carbon or glass fiber composites. For example, an incident angular beam spread of ±14° will excite all phase-match angles (below the shear critical angle) in a Plexiglas plate. Any higher incident angle produces total reflection back into the generation medium (air). On the other hand, a Type II transducer has 50±0.1 mm radius of curvature and active angular sensitivity of ±33° with respect to the normal axis. This arrangement provides approximately 50.8 mm (or about 2 inches) of geometric focal length. It is useful for either materials inspection or imaging applications in a wider range of materials because of the higher numerical aperture. Because high precision in the shape of the curved backplate fixture is not required, we have machined them using a conventional CNC machine. Thereafter, a 2-μm diameter aluminum oxide polish is used to bring the surface to a high finish.

Research towards a focused capacitive film transducer has been complicated by the installation of the metalized polymer film on a curved backplate, which produces many wrinkles in an unprepared film. Such wrinkles would compromise the performance characteristics of the device. This effect is far more severe for a large spherically focused capacitive air-coupled transducer. Previous authors have had to content themselves with backplate geometries that demand no deformation of the Mylar film [26, 27].

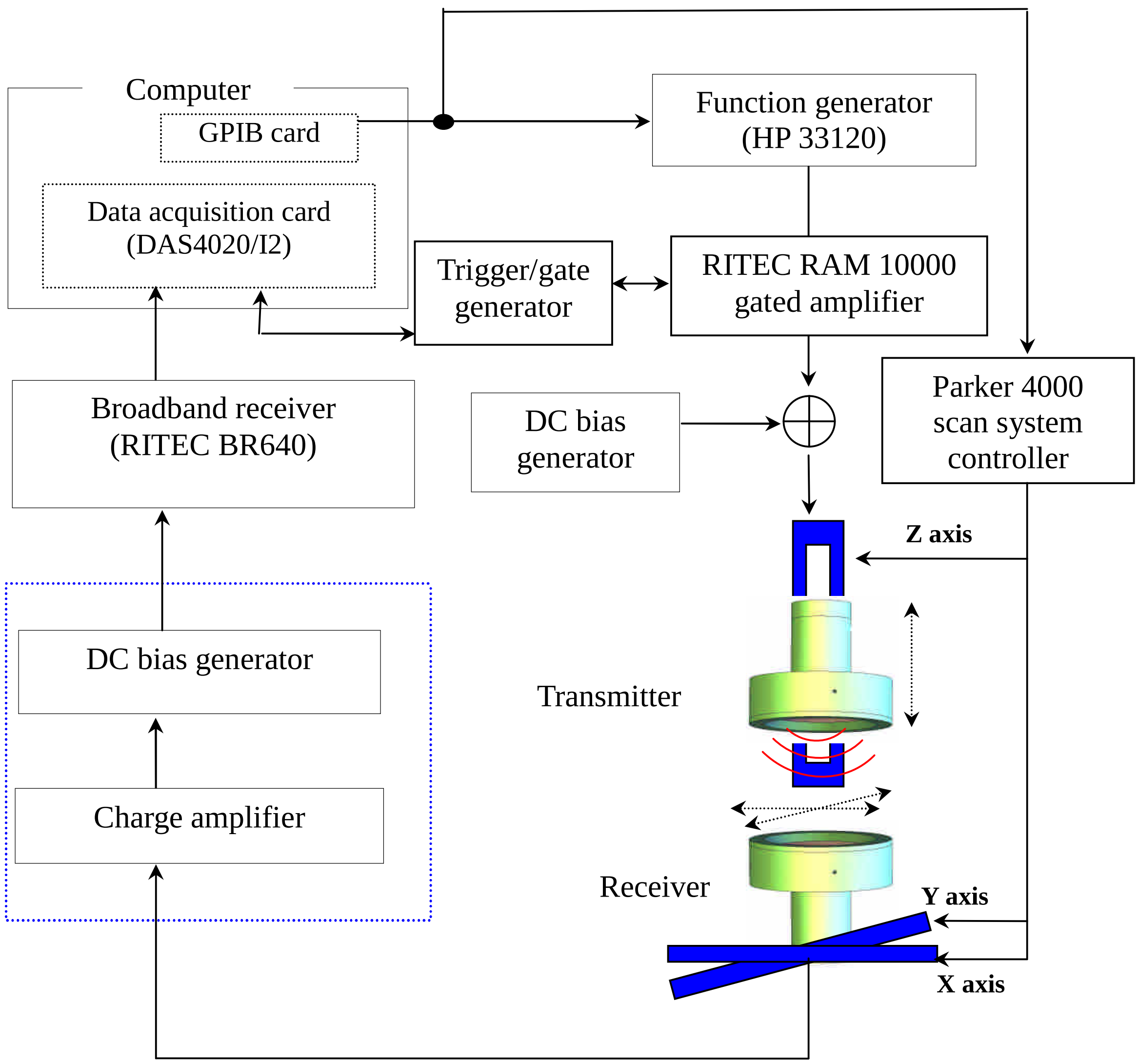

Figure 3. Simplified schematic diagram of the experimental setup for capacitive air-coupled ultrasound measurements.

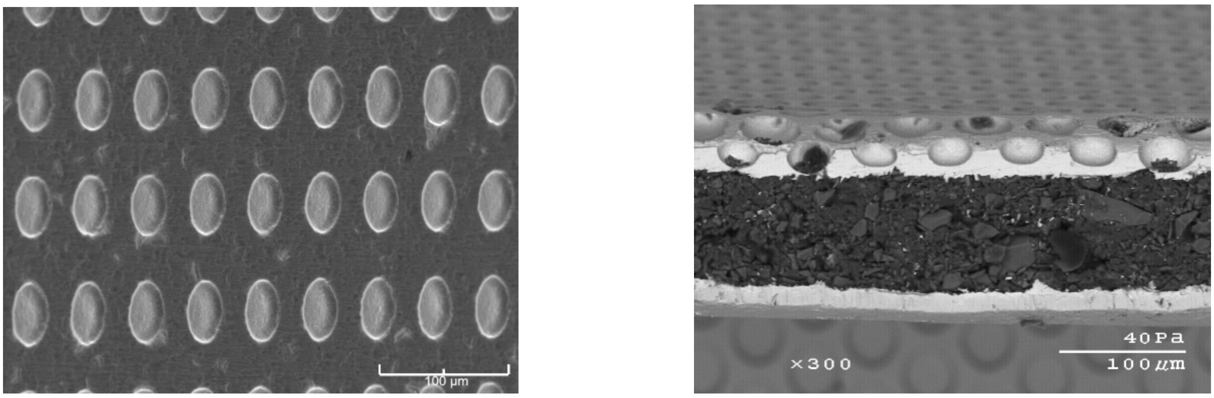

(a) (b)

Figure 4. (a) SEM image of a copper(Cu)/polyimide(PI) backplate (b) Cross-sectional SEM image of a Cu/PI backplate. The patterns are 40-μm in diameter and 80-μm center-to-center spacing between adjacent pits.

The primary cause of the wrinkles is the in-plane tensile rigidity of a polymer film. Even though a very thin polymer film is used with a very small flexural modulus, its tensile modulus is large enough that we cannot avoid wrinkles unless we treat the polymer film mechanically or chemically. The fabrication of a conformal polymer film was a major obstacle to be overcome when we sought to construct a focused capacitive air-coupled transducer, together with the fabrication of a curved backplate.

In order to solve this problem, we have developed a simple and easily applied process that completely suppresses all wrinkles in a Mylar film placed on a spherically curved backplate. To accomplish this objective, we have used a polished stainless steel ball bearing to gently stretch the metalized Mylar film. The radius of the steel ball bearing is approximately the same as the geometric focal length of a spherically focused capacitive transducer. For the Type I transducers we have used a 1-inch radius stainless steel ball bearing, and a 2-inch for the Type II device.

After stretching the film for about 20 to 30 seconds, the resulting film becomes semi-spherical, like a counterpart of the spherical backplate, where the polymer side is facing to the backplate. When attaching the Mylar film on the spherically curved backplate, we apply about 20 or 30 Vdc bias to the transducer. This simple and easy process works with high reliability, regardless of the film thickness, up to 12.5 μm. For instance, we have successfully stretched a 12.5-μm thick Kapton film in a perfectly spherical conforming shape. In addition, this method is far better and more efficient than other methods we have tried to spherically deform Mylar films. Figure 5 shows photographs of Mylar films applied to Type I and II transducers. There is no significant wrinkle on either film. The cross-sectional views and fully constructed images for a 10-mm and 50-mm diameter spherically focused transducers are shown in Figure 6.

4. Results and discussion

A series of experiments has been conducted to characterize the spherically focused capacitive transducers we have designed and built. We have measured and predicted radiated beam patterns from beam diameter, focal length, frequency, and sound speed in air. In order to demonstrate its focusing capability, we have performed several trial scans on composite honeycomb, wood, and very thin wire.

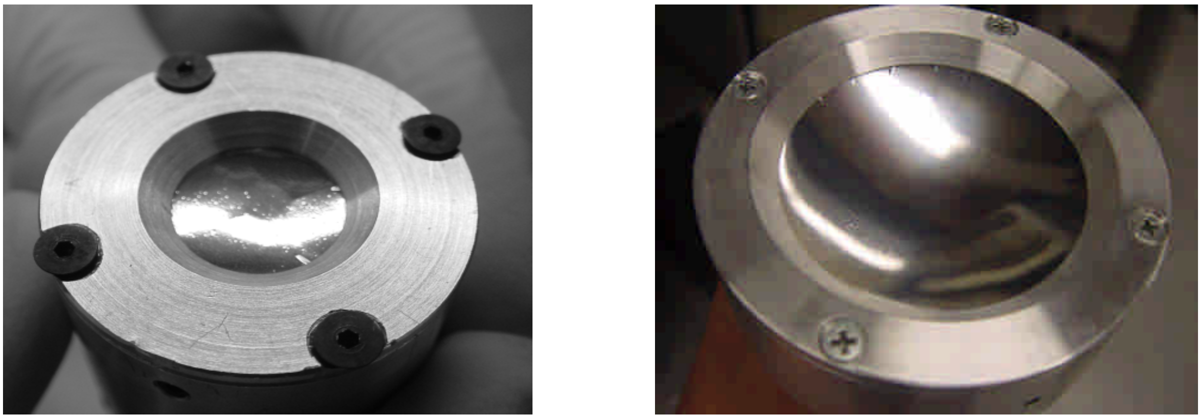

(a) (b)

Figure 5. Photographs of spherically conformed Mylar films deployed on focused capacitive air-coupled transducers, showing almost total absence of film wrinkling; (a) Type I and (b) Type II.

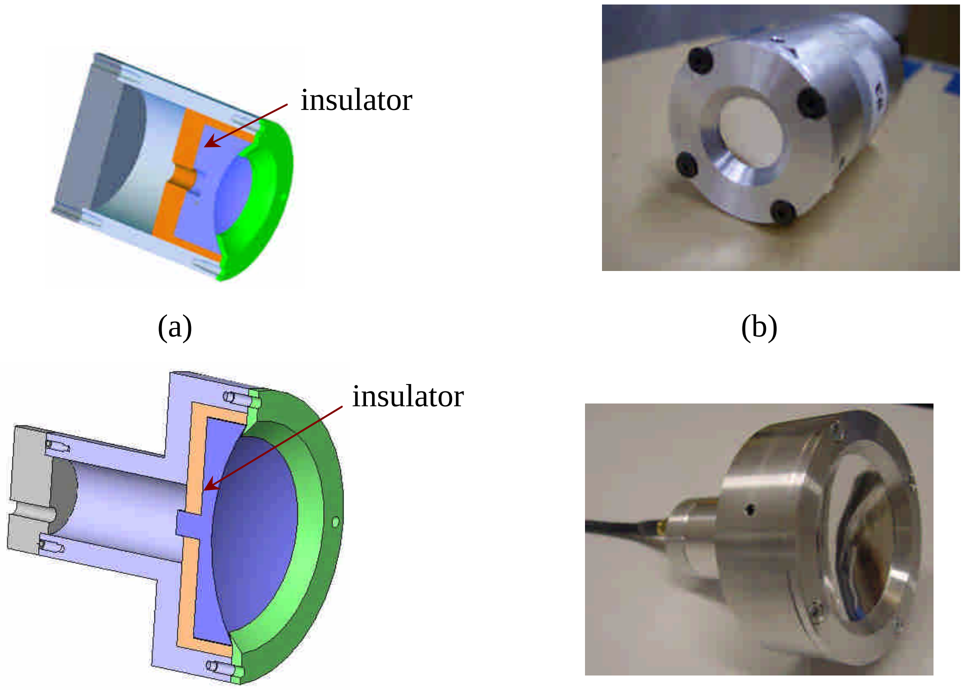

(a) (b)

(c) (d)

Figure 6. Cross-sectional diagrams and images of fully constructed Type I (a,b) and Type II transducers (c,d). A Type I has 10-mm diameter and 25.4-mm geometric focal length. A Type II has a 50.8-mm diameter and 50.8-mm geometric focal length. The transducers are made of aluminum, except the insulator. The insulator is fabricated from Delrin.

Using a quasi-point receiver (collimated planar air-coupled transducer) and focused transmitter, either a Type I or II transducer, the two are coaxially aligned and placed so that they face each other. The receiver-transmitter distance is carefully set at the point where the received signal amplitude shows the maximum. Depending on the focal length of a spherically focused capacitive transducer, it is observed that the distance can vary from the geometric focal length.

Figure 7(a) shows typical response of a Type II transducer when specific experimental conditions are used, such as 6-μm metalized Mylar film with a 100-nm thick aluminum layer coated on one side, 200 Vdc is applied to a quasi point receiver, and 250 V peak-to-peak transient signals are applied to a transmitter. It is shown that the time of arrival of the reflected waveform is approximately 149.3 μsec, which corresponds to a distance of 50.76 mm in air, assuming a sound velocity is 340 m/s in air. It is very close to the geometric focal length of a Type II transducer, which is 50.8 mm (= 2 inch). A more detailed study will be presented in the following sections. Figure 7(b) shows a corresponding frequency spectrum centered at 805 kHz with a bandwidth of approximately 800 kHz, which is measured at a lower and upper frequency of 400 and 1200 kHz, respectively. The wiggles are caused by the diffractions in the quasi-point receiver. We have observed a very similar frequency spectrum for the Type I device. As discussed later, the frequency characteristics are affected by various experimental conditions.

Note that, in addition to the transducer operating conditions, the propagation distance of an ultrasound in air can be accompanied by significant attenuation in the received signals. This attenuation can be predicted by [37]

$$\alpha_{cr} = 15.895 \times 10^{-11} \frac{(T/T_0)^{1/2}}{(P/P_0)} f^2, \quad \text{dB/m} \qquad (5)$$

where T is the measured temperature, T_0 is the room temperature in K, P is the measured pressure, P_0 is the atmosphere pressure, and f is the frequency of the signal. For example, the attenuation signal at the frequency 800 kHz through 5 cm of air under the standard conditions, i.e. $T=T_0$ and $P=P_0$, can be calculated by Equation (5), and the resulting attenuation is 5.17 dB, which is not even a factor of two.

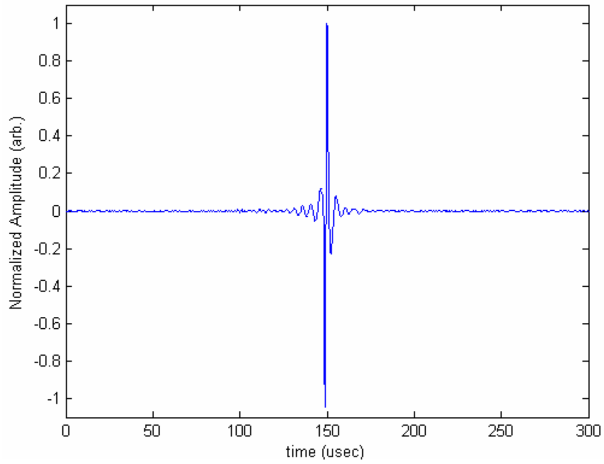

(a)

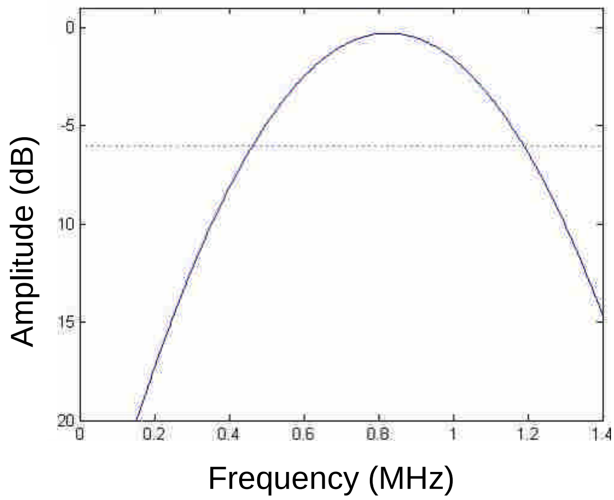

(b)

Figure 7. Typical amplitude response and corresponding frequency spectrum in a confocal configuration for a Type II transducer: (a) normalized signal amplitude, and (b) corresponding frequency spectrum. The quasi-point receiver is applied at 200 dc V, and the transmitter is driven by a broadband excitation (chirp) at 250 V peak-to-peak.

4.1. Transducer characterization

The sound fields radiated from Type I and II transducers are measured and compared to the theoretical predictions. Before the experiments start, the quasi-point receiver and transmitter, either a Type I or II transducer, are carefully aligned in parallel and placed in a confocal configuration. To perform logical and consistent transducer characterization, we have defined a simple Cartesian coordinate system as shown in Figure 8. The origin of the coordinate system is located at the center of the concave face of the spherical backplate in a Type I or II transducer. The theoretical sound field of an ideal spherically focused transducer is obtained using the O'Neil model, which is a modified Rayleigh-Somerfeld model. At the focal zone, this model shows that radiating sound pressure, p, in a fluid from a circular piston transducer of radius, a, having uniform piston velocity v_0 can be written as a Bessel function,

$$p(R_0, y, \omega) = -i\rho\omega v_0 a^2 \frac{\exp(ik\overline{R}_0)}{\overline{R}_0} \frac{J_1(kay/\overline{R}_0)}{kay/\overline{R}_0} \quad (6)$$

where R_0 is the focal length, $\overline{R}_0 = \sqrt{R_0^2 + y^2}$, k is the wave number, ρ is the density, y is the radial distance, and J_1 is the first order Bessel function.

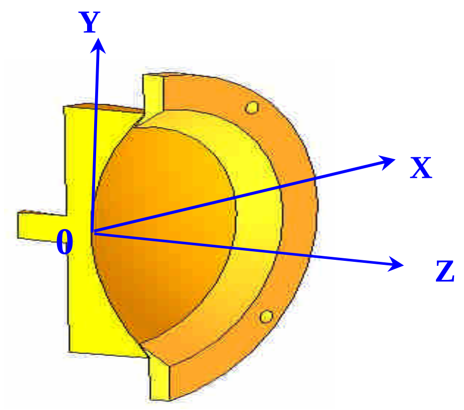

Figure 8. Coordinate system used in the transducer characterization.

4.2. 10-mm transducer

Figures 9 through 11 show the measured sound fields and theoretical predictions in the x-z plane at $y=0$, radiated from a 10-mm diameter spherically focused capacitive air-coupled transducer whose geometric focal length is 25.4 mm. The sound field is scanned in the x-z plane over an area of 8 mm x 40 mm and with spatial resolutions of 0.1 mm and 0.2 mm in the x- and z-axis, respectively. The precise position control is achieved by the computer controlled Parker-Daedel system. In order to obtain better insight into the field radiated from the transducer, measurements are made using three excitation signals: 500 kHz and 800 kHz tone burst, and broadband excitation (100 to 1500 kHz). The figures show peak-to-peak sound field amplitudes at each point where a darker red region represents much stronger sound field amplitude than a dark blue region.

Figure 9 shows the scanning results as the transducer is driven by a 500 kHz tone burst excitation. The maximum amplitude is measured at z=18.4 mm, compared to the theoretical prediction of 18.25 mm. The focal zone (or 6-dB drop-off points) is observed between 12.5 mm and 33.4 mm. It is very close to the theoretical predictions of 12.3 and 37.82 mm. Similarly, when it is driven by 800 kHz tone burst, shown in Figure 10, the maximum amplitude is measured at z=21.6 mm, while the theoretical prediction is 21.5 mm. Its focal zone is measured between 17.4 mm and 32.1 mm, compared to the theoretical prediction of 15.6 and 36.8 mm. For broadband excitation, the maximum amplitude and focal zone are measured at 24.9 mm and 17.1 and 34.1 mm, respectively. The calculated focal lengths of the Type I transducer are 18.4 mm, 21.6 mm and 24.9 mm for 500 kHz tone burst, 800 kHz tone burst, and broadband excitation. The theoretical predictions are sufficiently close to the experimental measurements for us to conclude that our device is operating like an ideal spherically focused piston radiator.

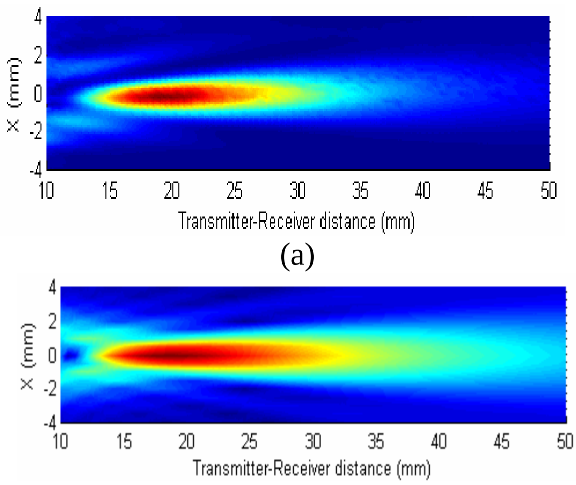

Figure 9. Measured sound pressure field (a) and theoretical prediction (b) in the *x-z* plane radiated from a 10-mm diameter, 25.4-mm focal length spherically focused air-coupled transducer driven by 500 kHz tone burst. The focal zone at -6 dB is approximately 12.5–33.4 mm. The maximum amplitude is measured at 18.4 mm, compared to the theoretical prediction of 18.3 mm. Darker red regions represent much stronger sound pressure fields than dark blue regions.

Figure 10(b) shows the cross sections of the focal region of the measured and theoretical sound pressure fields radiated from the 10 mm diameter transducer. The theoretical sound pressure field is calculated by Equation (6). The measurements are obtained at the focal zone for each excitation signal, which we have found in the *x-z* plane scan. For the 500 kHz tone burst excitation shown in Figure 9, the full width at half maximum (FWHM) value, or 6-dB drop-off point, is approximately 2.61 mm, compared to the theoretical prediction of 2.58 mm. There is small amplitude difference in the side lobes between measurements and theoretical predictions. This difference resulted from the misalignments in the receiver and transmitter since we manually control their leveling. This can be improved by aligning both the receiver and transmitter more accurately. For the 800 kHz tone burst excitation, the FWHM value is measured to be 1.38 mm, and its theoretical prediction is 1.37 mm as shown in Figure 10. Owing to better alignments between the quasi-point receiver and transmitter, the measurements are shown to have good agreement with theoretical predictions in the side lobes, as shown in Figures 11 and 12. When the transducer is driven by a broadband excitation signal (100 to 1500 kHz), the measured FWHM value is approximately 2.7 mm at the focal point, z=24.9 mm. So the focal zone beam diameters of the Type I transducer are 2.61 mm, 1.38 mm, and 2.7 mm for 500 kHz tone burst, 800 kHz tone burst and broadband excitation. There is no significant difference from an ideal spherically focused piston transducer's beam diameter.

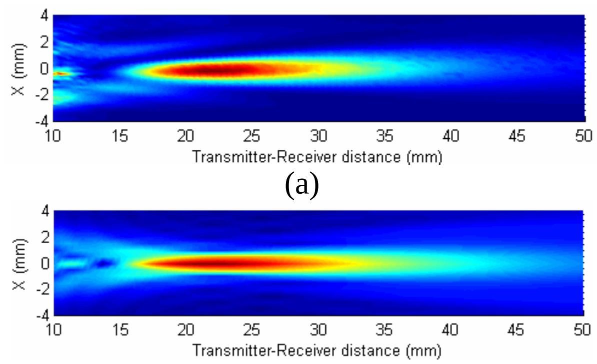

Figure 10. Measured sound pressure field (a) and theoretical prediction (b) in the *x-z* plane radiated from a 10-mm device driven by an 800 kHz tone burst. The focal zone at -6 dB is approximately 17.4 to 32.1 mm. The maximum amplitude is measured at 21.6 mm, compared to the theoretical estimate of 21.5 mm.

4.3. 50-mm transducer

Similar to the Type I, 10-mm transducer, we have performed the same experiments to determine the true focal length of a 50 mm diameter spherically focused capacitive air-coupled transducer whose geometric focal length is 50.8 mm (about 2 inches). Figures 13 and 14 show the measured sound fields and theoretical predictions in the *x*-*z* plane at *y* = 0. The theoretical sound pressure is calculated by the O'Neil model [37]. The sound field is scanned in the *x*-*z* plane over an area of 4 mm x 60 mm and with spatial resolutions of 0.05 mm and 0.2 mm in the *x*- and *z*-axis, respectively. Measurements are also made using two excitation signals; 500 kHz and a broadband excitation (100 to 1500 kHz). The figures show peak-to-peak sound field amplitude at each point where a darker red region represents much stronger sound field amplitude than a dark blue region. Figure 13 shows the scanning results for a 500 kHz tone burst excitation. We find the maximum amplitude at *z*=50.55 mm, compared to the theoretical prediction of 50.6 mm. The focal zone (6-dB drop-off points) is observed between 47.7 mm and 54.3 mm, very close to the theoretical predictions of 47.6 to 54.15 mm. For the broadband excitation, the maximum amplitude and focal zone are found at 50.7 mm and 46 to 57 mm, respectively. The focal lengths of the Type II transducer computed according to physical acoustics are 50.55 mm for 500 kHz tone burst and 50.7 mm for the broadband excitation, which are acceptably close to the calculation. Therefore, we conclude that the transducer is operating as an ideal spherically focused piston radiator.

Figure 15 shows the measured and theoretical sound pressure field cross sections in the focal region from a 25.4 mm radius, 50.8 mm focal length spherically focused air-coupled transducer excited by a 800-kHz tone burst. The theoretical sound pressure is calculated by Equation (6). For a 500 kHz tone burst, the full width at half maximum (FWHM) value, or 6-dB drop-off points, is approximately 0.94 mm, compared to the theoretical prediction of 0.938 mm. Similarly, for the 800 kHz tone burst excitation, the FWHM value is measured approximately

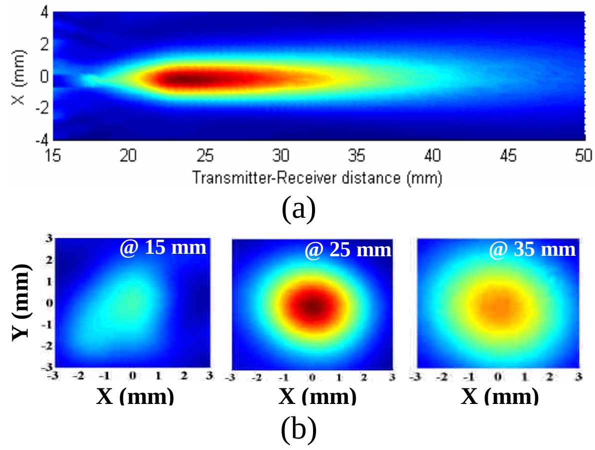

Figure 11. Measured sagittal (a) and cross-section (b) sound pressure fields radiated by the 10-mm focused radiator driven by a broadband transient signal. The focal zone at -6 dB is approximately 17.1 to 34.1 mm. The maximum amplitude is measured at 24.9 mm. Darker red regions represent much stronger sound pressure fields than dark blue regions.

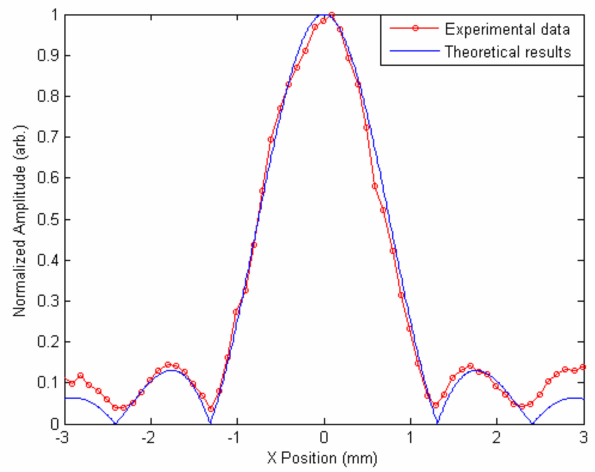

Figure 12. Cross section of the focal plane (*z*=21.5 mm) for the measured and theoretical sound pressure fields radiated from a 10-mm diameter, 25.4 mm focal length spherically focused air-coupled transducer when driven by 800 kHz tone burst excitations. The width of the measured sound fields at a half maximum (or 6-dB drop-off points) is approximately 1.38 mm, compared to the theoretical estimate of 1.37 mm.

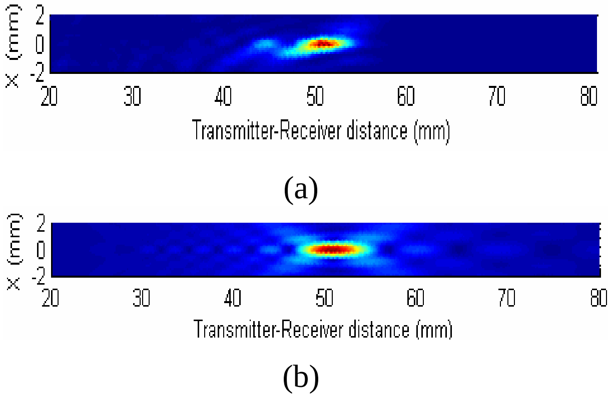

Figure 13. Measured sound pressure field (a) and theoretical prediction (b) in the *x-z* plane radiated from a 25.4-mm radius, 50.8-mm focal length driven by 500 kHz tone-burst. The focal zone (or 6-dB drop-off points) is approximately 47.7–54.3 mm. The maximum amplitude is measured at 50.55 mm (about 2 inches). Darker red regions represent much stronger sound pressure fields than dark blue regions.

0.71 mm and its theoretical prediction is 0.708 mm. When the transducer is driven by broadband excitation signal (100 to 1500 kHz), the measured FWHM value is approximately 1.32 mm at the focal point, z=50.7 mm. The calculated beam diameter (at -6 dB) of the Type II transducer is 1.32 mm for broadband excitation. The observed asymmetry in some plots is caused, we believe, by imperfect misalignment between the receiver and transmitter, which can be attributed to the limitations of our transducer positioning. Because wavelengths are short in air, transducer alignment is critical to the measurement of accurate results.

4.4. Applications to ultrasonic NDE

To demonstrate the spatial resolution and C-scan imaging performance of our new transducers, identical pairs of either 10-mm or 50-mm devices have been used to scan or image various samples in a confocal, through-transmission configuration. Both sets of transducers employ 6 μm thick aluminized Mylar films. On the receiver side a 300 Vdc bias is applied. The transmitter is driven by a 1 MHz tone burst at a dc bias of 250 V_{pp}. Figure 16(a) shows a 2-dimension C-scan image produced by scanning a thin wire (diameter = 340.0 ± 2.0 μm) over an area of 1 x 5 mm and with a spatial resolution of 0.01 mm. The black region represents the image of the wire. Figures 16(b) and (c) show the normalized peak-to-peak signal amplitude measured across the wire and its corresponding frequency response. The measurements show that the diameter of the wire is 254 μm, as judged by taking the difference of the lateral positions at 6-dB higher than the minimum. Based on these experimental results, we hypothesize that the Type II (50-mm) transducer is capable of an image resolution of about 130-μm in broadband excitation.

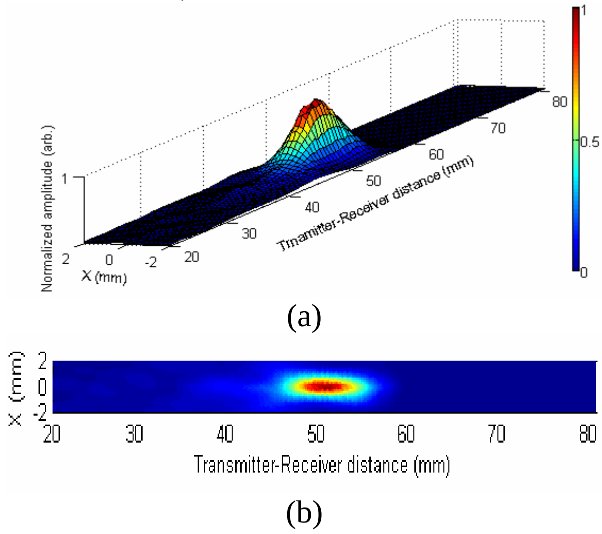

Figure 14. Measured sound pressure fields radiated from a 25.4-mm (1 inch) radius, 50.8-mm (2 inches) focal length driven by broadband transient signals. The focal zone (or 6-dB drop-off points) is approximately 46–57 mm. The maximum amplitude is measured at 50.7 mm (≈ 2 inches). Darker red regions represent much stronger sound pressure fields than dark blue regions.

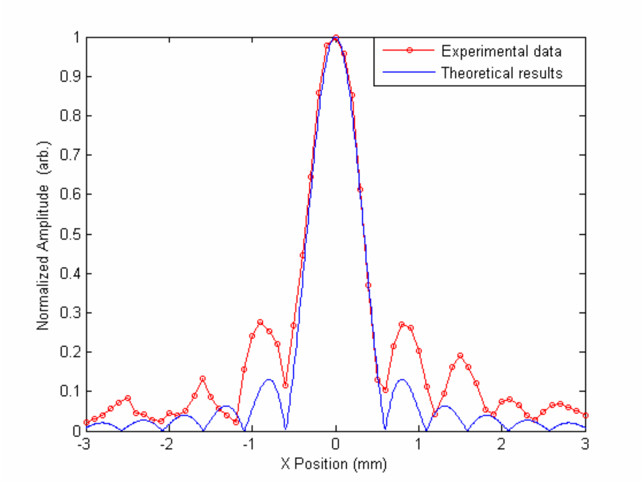

Figure 15. Cross sections of measured and theoretical sound pressure field amplitudes in the focal region (z=50.8 mm) of a 25.4-mm radius, 50.8-mm focal length spherically focused air-coupled transducer when driven by an 800 kHz tone burst excitation. The vertical scale units are arbitrary and the experimental curve is normalized to the peak of the calculation. The width of the measured sound fields at a half maximum (or 6-dB drop-off points) is approximately 0.71 mm, compared to a theoretical estimate of 0.708 mm.

Figure 17(a) shows the result of scanning with a pair of the 10-mm transducers in broadband excitation on a sample of honeycomb-core structural material with composite facesheets. Embedded into the composite/honeycomb are composite inserts, as illustrated in Figure 17(b). The C-scan, performed with the Type I devices in a confocal through-transmission geometry, clearly images all significant structure in the sample, including the texture of the woven graphite-epoxy composite facesheets. The inserts and their bonding to the facesheets are also well imaged in this figure.

Figures 18(a) and (b) show a photograph and air-coupled C-scan image of a natural material, balsa wood core, using the 10-mm transducers in broadband excitation. This material is fabricated as the 25-mm thick core of a marine composite to be finished with glass-epoxy facesheets. In the C-scan image we can see both the natural ring growth

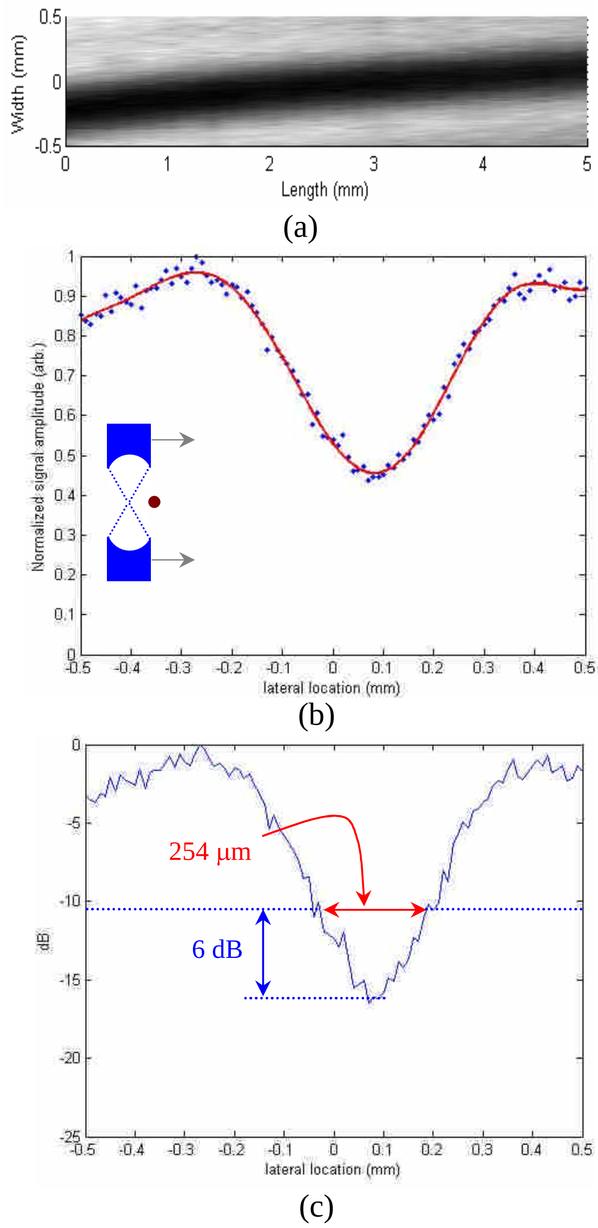

Figure 16. (a) A 2-dimension scan image of a copper wire. The dark black line represents the wire. (b) Normalized peak-to-peak signal amplitude measured across a copper wire, and (c) Corresponding frequency response. The diameter of the wire is approximately 250±2.0 μm.

structure, as well as several internal naturally occurring defects. The bondline between sections of the vertical-grain balsa wood is clearly visible at the right edge of the image.

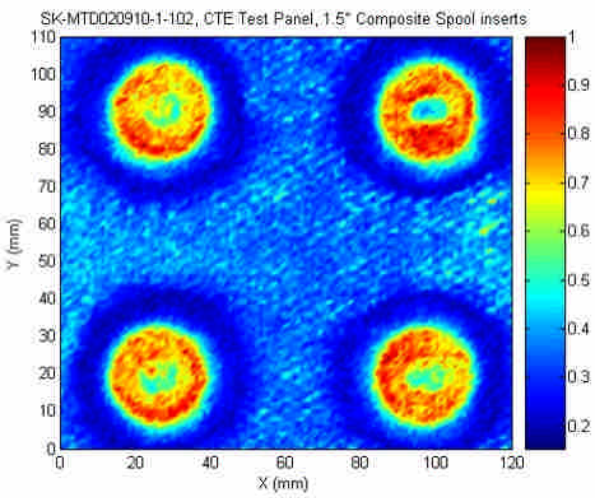

(a)

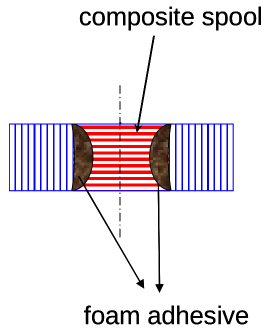

(b)

Figure 17. (a) Air-coupled confocal C-scan with 10-mm transducers of composite facesheet/honeycomb samples with inserts, showing texture in composite facesheet and details of bonding of spool inserts to facesheets; (b) geometry of composite spool inserts.

5. Conclusions

We have designed, fabricated, and characterized two different types of spherically focused capacitive air-coupled transducers for the first time. One has a 10-mm diameter and 25.4-mm geometric focal length, and the other has a 50-mm diameter and 50.8 mm geometric focal length. The key element that permits the simple fabrication of our transducers is a *flexible* copper/polyimide circuit board material, which we have employed as a backplate in place of the conventional silicon substrate. Utilizing its deformability and ease of microfabrication, we have demonstrated that spherically focused air-coupled ultrasonic probes can be made to function without the need of an external focusing device, such as a zone plate or an acoustic mirror. In addition, our focused capacitive transducer can be constructed with any backplate shape, permitting any type of spherical, bi-radial, or cylindrical focused or defocused beam. The flexible backplate further assures us of low fabrication cost and time. We have also invented a simple and easily applied method to conform the metalized polymer film onto a spherically curved backplate, while suppressing wrinkling on the film. Both spherically focused capacitive transducers have frequency spectra centered at 805 kHz with –6-dB points at 400 kHz and 1200 kHz. The measured behavior is compared to the theoretical predictions based on physical acoustics calculations. Good agree-

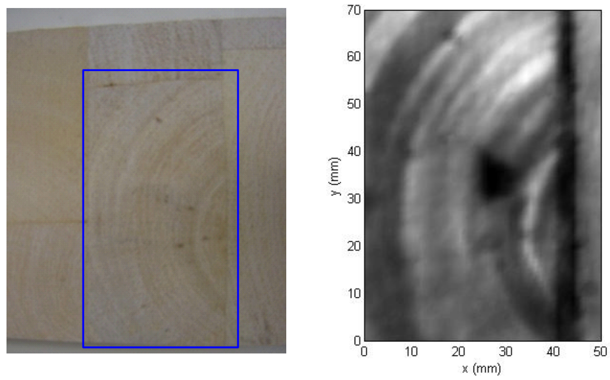

Figure 18. (a) photograph of balsa wood core of a marine composite, where blue rectangle shows area scanned in C-scan image; (b) air-coupled C-scan of balsa wood performed using 10-mm transducers in broadband excitation.

ment has been shown between measurement and theory, suggesting that our probes behave as ideal spherically focused piston transducers. We have demonstrated the imaging and NDE capabilities of these new devices through two C-scan images and by imaging a 250 μm diameter copper wire.

References

[1] Chimenti, D. E. and C. M. Fortunko. 1994. Characterization of composite prepreg with gas-coupled ultrasonics. *Ultrasonics*, 32: 261-264.

[2] Castaings, M., P. Cawley, R. Farlow, and G. Hayward. 1998. Single sided inspection of composite material using air-coupled ultrasound. *Journal of Nondestructive Evaluation*, 17: 37-45.

[3] Ergun, A.S., A. Atalar, B. Temelkuran, and E. Ozbay. 1998. A sensitive detection method for capacitive ultrasonic transducers. *Applied Physics Letters*, 72(23): 2957-2959.

[4] Kelly, S. P., G. Hayward, and T. E. Gomez. 2001. An air-coupled ultrasonic matching layer employing half wavelength cavity resonance. *Proceedings, IEEE Ultrasonics Symposium*: 965-967.

[5] Kraub, O., R. Gerlach, and J. Fricke. 1994. Experimental and theoretical investigations of SiO_2-aerogel matched piezo-transducers. *Ultrasonics*, 32(3): 217-222.

[6] Reily, D. and G. Hayward. 1991. Through air transmission for ultrasonic nondestructive testing. *Proceedings, IEEE Ultrasonics Symposium*: 763-766.

[7] M. Rafiq and C. Wykes. 1991. The performances of capacitive ultrasonic transducers using v-grooved backplate. *Measurement Science & Technology*, 2: 168-174,

[8] Schindel, D.W., D.A. Hutchins, L. Zou, and M. Sayer. 1995. The Design and Characterization of Micromachined Air-Coupled Transducer Capacitance. *IEEE Transactions on Ultrasonics Ferroelectrics And Frequency Control*, 42(1): 42-50.

[9] Haller, M. I. and B. T. Khuri-Yakub. 1996. A surface micromachined electrostatic ultrasonic air transducer. *IEEE Transactions on Ultrasonics Ferroelectrics And Frequency Control*, 43(1): 1-6.

[10] Ladabaum, I., B. T. Khuri-Yakub, and D. Spoliansky. 1996. Micromachined ultrasonic transducers: 11.4 MHz transmission in air and more. *Applied Physics Letters*, 68(1): 7-9.

[11] Jin, X., I. Ladabaum, F. L. Degertekin, S. Calmes, and B. T. Khuri-yakub. 1999. Fabrication and characterization of surface micromachined capacitive ultrasonic immersion transducers. *IEEE Journal of MEMS*, 8(10): 100-114.

[12] Carr, H. and C. Wykes. 1993. The performance of capacitive transducers, *Ultrasonics*, 31: 13-20.

[13] Suzuki, K., K. Higuchi, and H. Tanigawa. 1999.A Silicon Electrostatic Ultrasonic Transducer. *IEEE Transactions on Ultrasonics Ferroelectrics And Frequency Control*, 36(6): 620-627.

[14] Hietanen, J., J. Stor-Pellinen, and M. Luukkala. 1992. A model for an electrostatic ultrasonic transducer with a grooved backplate. *Measurement Science & Technology*, 3: 1095-1097.

[15] McIntyre, C. S., D.A. Hutchins, D. R. Billson, and J. Stor-Pellinen. 2001. The use of air-coupled ultrasound to test paper. *IEEE Transactions on Ultrasonics Ferroelectrics And Frequency Control*, 48(3): 717-727.

[16] Schindel, D. W. 1999. Air-coupled ultrasonic measurements of adhesively bonded multi-layer structures. *Ultrasonics*, 37: 185-200.

[17] Safaeinili, A., O. I. Lobkis, and D. E. Chimenti. 1995. Air-coupled ultrasonic estimation of viscoelastic stiffnesses in plates. *IEEE Transactions on Ultrason-*

ics Ferroelectrics And Frequency Control, 43: 1171-1180.

[18] Badi, M. H., G. G. Yaralioglu, A. S. Ergun, S. T. Hansen, E. J. Wong, and B. T. Khuri-Yakub. 2003. Capacitive micromachined ultrasonic Lamb wave transducers using rectangular membrane. *IEEE Transactions on Ultrasonics Ferroelectrics And Frequency Control*, 50(9): 1191-1203.

[19] Holland, S. D., S. V. Telles, and D. E. Chimenti. 2004. Air-coupled, focused ultrasonic dispersion spectrum reconstruction in plates. *Journal of The Acoustical Society of America*, 115: 2866.

[20] Holland, S. D. and D. E. Chimenti. 2003. Air-coupled acoustic imaging with zero-group-velocity lamb modes. *Applied Physics Letters*, 83: 2704.

[21] Neild, A., D. A. Hutchins, and D. R. Billson. 2004. Imaging using air-coupled polymer-membrane capacitive ultrasonic arrays. *Ultrasonics*, 42: 859.

[22] Schindel, D. W., A. G. Bashford, and D. A. Hutchins. 1997. Focusing of ultrasonic waves in air using a micromachined Fresnel zone-plate. *Ultrasonics*, 35: 275-285.

[23] Gan, T. H., D. A. Hutchins, D. R. Billson, and D. W. Schindel. 2002. High-resolution air-coupled ultrasonic imaging of thin materials. *Proceedings, IEEE Ultrasonics Symposium*: 897-900.

[24] Hosten, B. and M. Castaings. 2002. Parabolic mirror and air-coupled transducer for multimodal plate wave detection. Review of Progress in QNDE, Vol. 22, Editors: D. O. Thompson and D. E. Chimenti, *Plenum*, New York: 1243-1250.

[25] Wang, H. and M. Toda. 1999. Curved PVDF Airborne Transducer. *IEEE Transactions on Ultrasonics Ferroelectrics And Frequency Control*, 46(6): 1375-11386.

[26] Robertson, T. J., D. A. Hutchins, and D. R. Billson. 2002. Capacitive air-coupled cylindrical transducers for ultrasonic imaging applications. *Measurement Science & Technology*, 13: 758-768.

[27] Hutchins, D. A., T. J. Robertson, D. R. Billson, and P. Solanki. 2003. A conical air-coupled capacitance transducer for surface imaging. *Ultrasonics*, 41: 163-173.

[28] Wong, K. A., S. Panda, and I. Ladabaum. 2003. Curved micromachined ultrasonic transducers. *Proceedings, IEEE Ultrasonics Symposium*, 1: 572-576.

[29] Caroti, A., R. Carotenuto, G. Caliano, and M. Pappalardo. 2004. The effects of membrane metallization in capacitive microfabricated ultrasonic transducers. *Journal of Acoustical Society of America*, 115, 2: 651-657.

[30] Bozkurt, A., L. Ladabaum, A. Atalar, and B. T. Khuri-Yakub. 1999. Theory and Analysis of Electrode size optimization for capacitive microfabricated ultrasonic transducers. *IEEE Transactions on Ultrasonics Ferroelectrics And Frequency Control*, 46(6): 1364-1374.

[31] Teles, S. V. 2004. *Ultrasonic guided waves in composite plates*. Thesis, Iowa State University, Ames, Iowa.

[32] Schedahl Co., www.schedahl.com.

[33] Kurtz, S. R. and R. A. Anderson. 1986. Properties of the metal-polymer interface observed with space-charge mapping techniques. *Journal of Applied Physics*, 60(2): 681-687.

[34] Kadowaki, K., S. Nashimoto, and I. Kitani. 2000. Measurement of Polarization Charge Density at the Interface between PET-film and Electrode with a Thin Air Layer by PEA Method. *Proceedings of the 6th International Conference of Properties and applications of Dielectric material*, 254-257.

[35] Kurtz, S. R. and R. A. Anderson. 1984. Direct observation of field-injected space charge in a metal-insulator-metal

structure. *Journal of Applied Physics*, 56(10), 2856-2863.

[36] Bass, H. E., L. C. Sutherland, J. E. Piercy, and L. B. Evans. 1984. *Absorption of sound by the atmosphere, Physical Acoustics: Principles and Methods*, Vol. XVII, Academic Press. 145-232.

[37] Schmerr, L. W., Jr. 1998. *Fundamentals of ultrasonic nondestructive evaluation – A modeling Approach*. Plenum Press: 181-197, New York, NY.